



Centella asiatica transfersomes and Bergamot essential oil nanoemulsion combined in gel exhibited anti-photoaging effects on UVB-radiated BALB/c mice

Ekowati Retnaningtyas^{a,*}, Budi Susatia^a, Husnul Khotimah^b, Achmad Rudijanto^c, Ahmed Ali Ahmed Abousouh^d, Andri Setiawan^d

^a Departement of Nursing, Malang State Health Polytechnic, Ministry of Health Indonesia, Malang 65119, Indonesia

^b Department of Pharmacology, Faculty of Medicine, Universitas Brawijaya, Malang 65145, Indonesia

^c Department of Internal Medicine, Faculty of Medicine, Universitas Brawijaya, Malang 65145, Indonesia

^d Master Program of Biomedical Sciences, Faculty of Medicine, Universitas Brawijaya, Malang 65145, Indonesia

ARTICLE INFO

Keywords:

Anti-photoaging
Bergamot essential oil
Centella asiatica
Nanoemulsion
Transfersomes
Ultraviolet radiation

ABSTRACT

Photoaging of skin tissue can result from exposure to ultraviolet B (UVB) radiation. This study developed two nanocarriers *Centella asiatica* (CA) transfersomes (TF) and Bergamot essential oil (BEO) nanoemulsions (NE) combined in a gel formulation as a drug delivery system, in order to study whether they could synergize to prevent UVB radiation and provide anti-photoaging effects. Nanoencapsulation of CA-TF and BEO-NE were examined for their quality by characterizing their physicochemical properties. An *in vivo* study evaluated topically applied CA-TF and BEO-NE combination gels biological effect on BALB/c mice before UVB radiation (840 mJ/cm²) for two weeks. Particle size analysis of developed nanocarriers exhibited monodispersed pattern with an average particle size and zeta potential of around 9.64 ± 0.35 nm and -39.86 ± 1.33 mV, respectively. *In vivo* experiments showed that topically applied CA-TF and BEO-NE combination gel significantly prevented UVB-induced wrinkle formation and skin erythema and inhibited histological damage, including epidermal hyperplasia, collagen fibers, and the destruction of elastic fibers. Additionally, the CA-TF and BEO-NE combination gel reduced UVB-induced oxidative stress by increasing superoxide dismutase (SOD) activity and suppressed lipid peroxidation by decreasing malondialdehyde (MDA) expression as well as inhibiting the expression of UVB-induced pro-inflammatory cytokines include tumor necrosis factor α (TNF- α) and interleukin 6 (IL-6). Moreover, the CA-TF and BEO-NE combination gel increased the type I collagen expression, restoring UVB-induced collagen production and density. Therefore, nanoencapsulation CA-TF and BEO-NE combination gel could synergistically prevent UVB-induced oxidative stress and inflammatory responses.

1. Introduction

People's life expectancy is rising along with their age and socio-economic development, and they are increasingly concerned about skin health because smooth skin can increase self-confidence (Maisel et al., 2018). Many skincare products have been investigated and developed, especially those that lead to the inhibition and delay of skin aging (Krutmann et al., 2021). Skin aging is divided into intrinsic age-related aging and ultraviolet B (UVB) radiation-induced photoaging. Photoaged skin's physiological and biochemical features include dehydration,

wrinkles, and increased epidermal thickness (Kammeyer and Luiten, 2015). A direct harmful impact of UVB radiation is the production of reactive oxygen species (ROS), which is associated with DNA damage and modification of gene expression. UVB radiation could accelerate the aging process by inducing photo-oxidation processes, particularly in the skin's epidermis, by upsetting the balance of enzymatic antioxidants in the skin, such as superoxide dismutase (SOD), catalase (CAT), and glutathione peroxidase (GSH-Px) (Lawrence et al., 2018). In addition, excessive ROS accumulation can increase the production of pro-inflammatory cytokines, including tumor necrosis factor α (TNF- α)

* Corresponding author.

E-mail addresses: ekowati_retnaningtyas@poltekkes-malang.ac.id (E. Retnaningtyas), budisusatia@poltekkes-malang.ac.id (B. Susatia), husnul_farmako.fk@ub.ac.id (H. Khotimah), achmadrudijanto@yahoo.co.id (A. Rudijanto), ahmedabusowa96@gmail.com (A. Ali Ahmed Abousouh), andre.bbc4088@gmail.com (A. Setiawan).

<https://doi.org/10.1016/j.jksus.2024.103207>

Received 26 October 2023; Received in revised form 21 March 2024; Accepted 9 April 2024

Available online 10 April 2024

1018-3647/© 2024 The Authors. Published by Elsevier B.V. on behalf of King Saud University. This is an open access article under the CC BY-NC-ND license (<http://creativecommons.org/licenses/by-nc-nd/4.0/>).

and interleukin 6 (IL-6), which directly regulate the activation of activator protein-1 (AP-1), modulation mitogen-activated protein kinases (MAPK) and nuclear factor-kappa B (NF- κ B) signaling pathways (Gu et al., 2020; Ansary et al., 2021; Wang et al., 2019). Excessive ROS production and inflammatory cytokines trigger the expression of matrix metalloproteinases (MMPs), further degrading the skin's extracellular matrix (ECM). This effect ultimately leads to collagen degradation in the ECM and the formation of skin photoaging (Laronha and Caldeira, 2020). Therefore, natural ingredients with antioxidant, anti-inflammatory, and collagen synthesis activities are considered an alternative to developing anti-aging skincare products (Hoang et al., 2021).

Centella asiatica L. Urban (CA), or Pegagan in Indonesia, is a herbal medicinal plant with high commercial value. This plant has been used in traditional medicine, and its broad ethnopharmacological activity has been applied in various cultures and countries, as evidenced in multiple studies (Belwal et al., 2019; Khotimah et al., 2022a). The main chemical components which could be responsible for dermatological and pharmacological activities include asiaticoside, madecassoside, asiatic acid, and madecassic acid (Bylka et al., 2014; Khotimah et al., 2021, 2022b). Besides CA, some essential oils from the peel of fruits, such as bergamot can also prevent skin aging due to their biological activity. *Bergamot essential oil* (BEO) is a crucial product widely used in many flavours and perfumes. BEO and its primary active ingredients, linalyl acetate, linalool, and limonene, have demonstrated anti-inflammatory, immunomodulatory, and wound-healing properties in various conditions (Dugo and Bonaccorsi, 2013; Keskin et al., 2017; Perna et al., 2019). CA and BEO have many beneficial pharmacological effects, making them potential candidates for skin damage prevention. However, preclinical and clinical applications of pharmacokinetics are limited by poor systemic absorption, resulting in low bioavailability (Bilia et al., 2014; Sun et al., 2020). Thus, we developed nanocarriers as topical drug delivery systems for CA and BEO to effectively transfer to the skin and ensure efficient penetration into the stratum corneum.

Transfersomes (TF) and nanoemulsions (NE) are vesicular nanocarriers whose surface is easily modified to increase penetration efficiency and effectiveness, protect against physicochemical instability, controlled release, and targeted delivery of active compounds (Mishra et al., 2018; Shukla et al., 2018). TF, also known as ultradeformable liposomes, are highly adaptable aggregates responsive to stress, self-regulating, and self-optimizing. TF is prepared by the addition of phospholipids and edge activators (EA) which make it more flexible and elastic, allowing it to penetrate the stratum corneum through intercellular lipid spaces, thereby increasing drug penetration and preventing vesicular rupture (El Zaafarany et al., 2010). On the other hand, NE are dispersions of oil-in-water (O/W) or water-in-oil (W/O) stabilized by surfactant(s), their average droplet size is in the range of 20 to 200 nm (Naseema et al., 2021; Souto et al., 2022).

This study aimed to develop two nanocarriers CA-TF and BEO-NE combined in a gel formulation as a topically applied drug delivery system capable of synergistically preventing and protecting UVB radiation and providing anti-photoaging effects. The physicochemical characteristics of nanocarriers were described using their zeta potential, polydispersity index, and particle size distribution. An optimized combination of TF and NE is incorporated into a gel form for a better topical application. Finally, the mechanisms underlying the preventive and protective activities of the CA-TF and BEO-NE combination gel were evaluated by macroscopic, histological, and immunohistochemical studies on oxidative stress and inflammation associated with photoaging using a UVB-induced BALB/c mice model.

2. Materials and methods

2.1. Plant preparations

UPT Materia Medica Batu City, East Java, Indonesia provided CA

fresh plants with 0.29 % asiaticoside concentration. They are washed with distilled water to remove contaminants, then dried, cut, and ground to obtain a fine powder. CA powder was extracted using the maceration method by adding 50 g of CA powder in 400 mL of 96 % v/v ethanol for 24 h. Then, the powder was filtered through filter paper with a pore size of 0.45 mm, and the ethanol extract was collected and concentrated by complete removal of the solvent using rotary evaporator (Khotimah et al., 2022b). Then, the concentrated extract was stored at -20°C in dark place for further experiments.

2.2. Production of TF, NE, and gel formulation

CA-TF were prepared by the thin-layer hydration method (El-Gizawy et al., 2020; Khotimah et al., 2022b). Concisely, the TF composition consisted of CA extract, Soya phosphatidylcholine (SPC) (Avanti Polar Lipids, Inc, Alabama, USA), Tween 80 (Sigma-Aldrich, Chemicals, Missouri, USA), and Phosphate buffer saline (PBS) pH 7.4. Precise weight measurements were used to dissolve Tween 80, SPC, and CA extract in 100 % methanol. The organic phase was evaporated for 60 min at 40°C and 50–150 rpm using a round-bottom flask and a rotary vacuum evaporator. A thin layer on the flask wall was formed after all the solvent had evaporated, then the lipid film hydration process was carried out by adding a PBS solution in vacuum for 60 min at 37°C and 100 rpm. The solid particles were then reduced in size by sonication for 10 min. All CA-TF suspensions were stored at 4°C until further analysis.

BEO-NE were prepared by low-energy methods (Khotimah et al., 2022b). Concisely, 25 g of Tween 80 was weighed, put into a beaker glass, and dissolved in 197.5 mL of distilled water. Then, the solution was homogenized for 5 min at 500 rpm. The speed was increased to 750 rpm for 10 min, after adding 25 g of propylene glycol. The hotplate was turned off, and the homogenizer was decelerated at 200 rpm. Add 2.5 mL of BEO (Young Living Essential Oils, Lehi, Utah) and stir again for 10 min. After cooling, NE was stored in a container at 4°C for further evaluation.

The CA-TF and BEO-NE combination gel for selected formulations was prepared with 1.25 g of Carbopol 940, dispersed in 198.25 mL of distilled water and stored in a dark place for 24 h so that Carbopol swelled completely. The next step was the formation of the Carbopol base gel by homogenizing the Carbopol using a homogenizer at 1500 rpm, and 0.5 g of Triethanolamine (TEA) was added slowly. After the gel was completely formed, the suspension (12.5 g, 25 g, and 50 g) of CA-TF and 25 g of BEO-NE was homogenized at 500 rpm for 15 min. The prepared gel formulation was stored at 4°C for further experiments.

2.3. CA-TF and BEO-NE characterization

These assessments were determined before incorporation of CA-TF and BEO-NE in gel form, by using the dynamic light scattering (DLS) method with a Zetasizer Nano ZS-90 (Malvern Instruments Ltd. UK) at 25°C and a scattering angle of 90° 24 h after preparation, the zeta potential, polydispersity index, and particle size distribution of produced CA-TF and BEO-NE were determined. The samples were diluted at 1:80 in distilled water to achieve the right count rate. This experiment used triplicates ($n = 3$) for all measures.

2.4. Animals and experimental design

The Pharmacology Laboratory of Universitas Brawijaya provided 24 male BALB/c mice (8 weeks, weight range 20–22 g) for the *in vivo* experiments. Mice were maintained under standard environmental conditions of $23 \pm 2^{\circ}\text{C}$ temperature, $50 \pm 10\%$ humidity, 12 h light/dark cycle, and free access to standard laboratory diet and water *ad libitum*. All animal experimental procedures and protocols were reviewed and approved by the Ethics Committee, Malang State Health Polytechnic, Indonesia (Number 033/KEPK-POLKESMA/2021). In addition, every effort has been made to minimize the number of animals used and to

reduce distress due to the procedures used in this study. After a week of acclimation, mice were randomly divided into 6 groups of 4 mice each. Before the experiment, the mice's dorsal skin area ($2 \times 2.5 \text{ cm}^2$) was shaved to remove any hair.

2.5. UVB radiation and gel application

The UVB light source was provided by a parallel array of two UVB lamps (25 W; wavelength range of 290–320 nm; Rolf C. Hagen Inc., CA, USA), used to examine the ability of CA-TF and BEO-NE combination gel to prevent and protect photoaging. The UVB radiation conditions and topical application of the gel used in this experiment replicated the previous study design and were modified with other agents because previous studies reported that a total UVB dose of 840 mJ/cm^2 for two weeks successfully caused skin photoaging in BALB/c mice model (Khotimah et al., 2022b). Topical application of CA-TF and BEO-NE combination gel on BALB/c mice's dorsal skins was performed 50 min before UVB radiation and applied evenly (2 g/mice) 3 times a week for 2 weeks. Table 1 displays the experimental schedule. Canon EOS 5D camera (Canon Inc., Tokyo, Japan) was used to observe and photograph areas on the dorsal skin of mice during the experiments. Visual skin changes in mice were evaluated through ImageJ 1.53e software. A skin photodamage scoring system assessed UVB-induced skin photoaging (Table 2) (Feng et al., 2014). After two weeks of experiments, the animals were sacrificed under intraperitoneal anesthesia. Then, the skin tissue was collected for further analysis.

2.6. Histological examinations

Mice's dorsal skin tissue was fixed for 24 h in a 4 % paraformaldehyde solution. Then, the slides performed xylene deparaffinization, were dehydrated using graded alcohol, paraffin-embedded, and then cut with a rotating microtome (Leica, Germany) to a thickness of 4 μm . The histological observation was performed with hematoxylin and eosin (HE) staining to evaluate the epidermal hyperplasia and Masson's trichrome to assess collagen deposition. Histological changes were examined under an optical microscope (Cx23, Olympus Inc., Tokyo, Japan) and quantified with ImageJ 1.53e software.

2.7. Immunohistochemistry analysis

Skin tissue slides were dehydrated through a graded ethanol series, and the antigen on the slide was recovered with citrate buffer for 3 min. Then, endogenous peroxidases in tissues were inactivated with 3 % hydrogen peroxide in PBS for 30 min. In subsequent steps, the slides were incubated with primary antibodies, including anti-SOD, anti-MDA, anti-TNF- α , anti-IL-6, and anti-type I collagen (1:200, from Santa Cruz Biotechnology, CA, USA) in a wet box at 4 °C overnight. Then, the slides were incubated with biotinylated secondary antibodies and followed by Strep Avidin-Horseradish Peroxidase (SAHRP) for 50 min each at 25 °C. Subsequently, the sections were dehydrated, mounted and examined at

Table 1
Experimental design groups.

Group	Experimental procedure
Control	Mice were untreated sample and not exposed to UVB (normal).
UVB	Mice were topically applied with 2 g of Carbopol base gel before UVB exposure
UVB + NTF 0.3 %	Mice were topically applied with 2 g of 0.3 % CA extract and 1 % BEO-NE combination gel before UVB exposure
UVB + TF 0.15 %	Mice were topically applied with 2 g of 0.15 % CA-TF and 1 % BEO-NE combination gel before UVB exposure
UVB + TF 0.3 %	Mice were topically applied with 2 g of 0.3 % CA-TF and 1 % BEO-NE combination gel before UVB exposure
UVB + TF 0.6 %	Mice were topically applied with 2 g of 0.6 % CA-TF and 1 % BEO-NE combination gel before UVB exposure

Table 2
Mice's skin photodamage scoring system.

Score	Skin appearance
0	Normal skin that appears smooth, pink, and plump.
0.5	The exposed site is displaying mild erythema.
1	Few scales, slight edema, and moderate erythema at the exposed spot.
1.5	Significant edema, noticeable erythema, scales, and slight roughness at the exposed spot.
2	Many scales, visible roughness, hypertrophy, and wrinkles at the exposed location are all present in the gray skin.

1000x magnification under an optical microscope (Cx23, Olympus Inc., Tokyo, Japan) and quantified with ImageJ 1.53e software.

2.8. Statistical analysis

Statistical analyses were performed with SPSS software (21.0. IBM Inc. USA). The data are shown as the mean \pm standard deviation. The data were subjected to one-way ANOVA with Tukey's post hoc test. A P-value < 0.05 was considered statistically significant.

3. Results

3.1. Physicochemical characterization of CA-TF and BEO-NE

DLS analysis reported the average particle sizes of CA-TF and BEO-NE as $49.98 \pm 5.67 \text{ nm}$ and $9.64 \pm 0.35 \text{ nm}$, respectively. The polydispersity index values for CA-TF and BEO-NE were 0.13 ± 0.03 and 0.19 ± 0.01 , respectively. The polydispersity index was less than 0.2, indicating that the CA-TF and BEO-NE developed had a narrow particle size distribution and were homogeneous. In addition, the nanocarriers CA-TF and BEO-NE were found to have a zeta potential value of $-30.87 \pm 1.91 \text{ mV}$ and $-39.86 \pm 1.33 \text{ mV}$, respectively, indicating good stability.

3.2. Effect of CA-TF and BEO-NE combination gel on macroscopic appearance

The representative photographs of the macroscopic appearance of mice skin in each group during the two weeks (Fig. 1.a). Mice in the control (normal) group that were only shaved but not exposed to UVB showed healthy, smooth, elastic, and no wrinkles dorsal skin, indicating that shaving did not cause macroscopic skin lesions. After 14 days of UVB induction (UVB group), on the surface of the mice's skin, erythema, wrinkles, dryness, roughness, and other signs were visible, showing that UVB exposure can cause skin photoaging in mice. In contrast, when the CA-non-TF and BEO-NE combination gel (UVB + NTF 0.3 % group) or the CA-TF and BEO-NE combination gel (UVB + TF 0.15 %, 0.3 %, and 0.6 % groups) topically applied, macroscopic skin changes due to UVB exposure could be prevented and ameliorated.

For two weeks, the UVB-induced dorsal skin of mice increased the formation of rough and deep wrinkles (UVB group), as shown in Fig. 1.b. In contrast, in the UVB + NTF 0.3 % group, UVB exposure, which resulted in wrinkle formation, was significantly inhibited compared to the UVB group ($p < 0.05$). Besides, the UVB + TF 0.15 %, 0.3 %, and 0.6 % groups significantly inhibited UVB-induced wrinkle parameters, resulting in reductions in wrinkle area, depth, length, and number of 50.1 %, 48.1 %, and 49.3 %, respectively, in comparison to values obtained for the UVB-induced group.

As shown in Fig. 1.c, compared with the control group, in the UVB group, the visual skin manifestations score significantly increased ($p < 0.05$) after 14 days of UVB exposure. Nevertheless, the UVB-induced skin macroscopic changes significantly ameliorated skin visual manifestation scores in the UVB + NTF 0.3 % group compared with UVB group. Moreover, with the topical application of the CA-TF and BEO-NE combination gel (all groups), the skin visual manifestation scores were

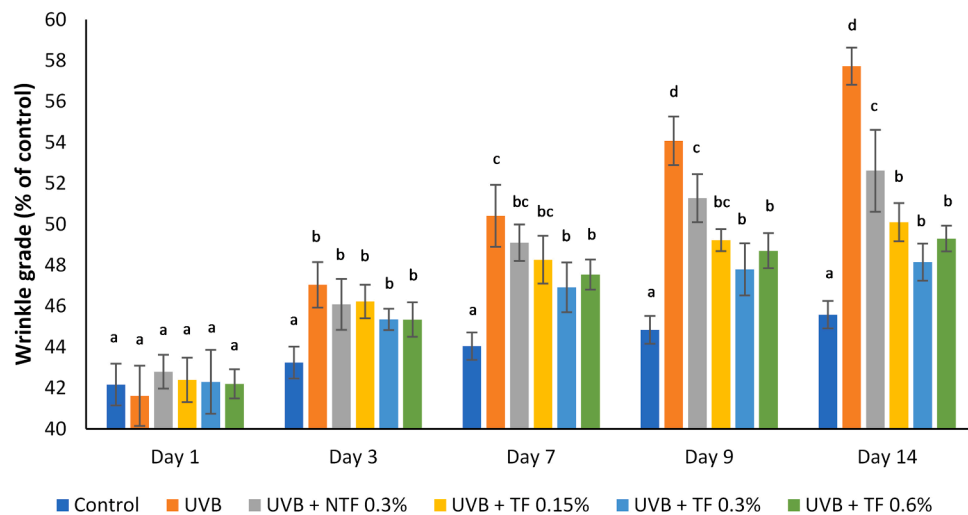
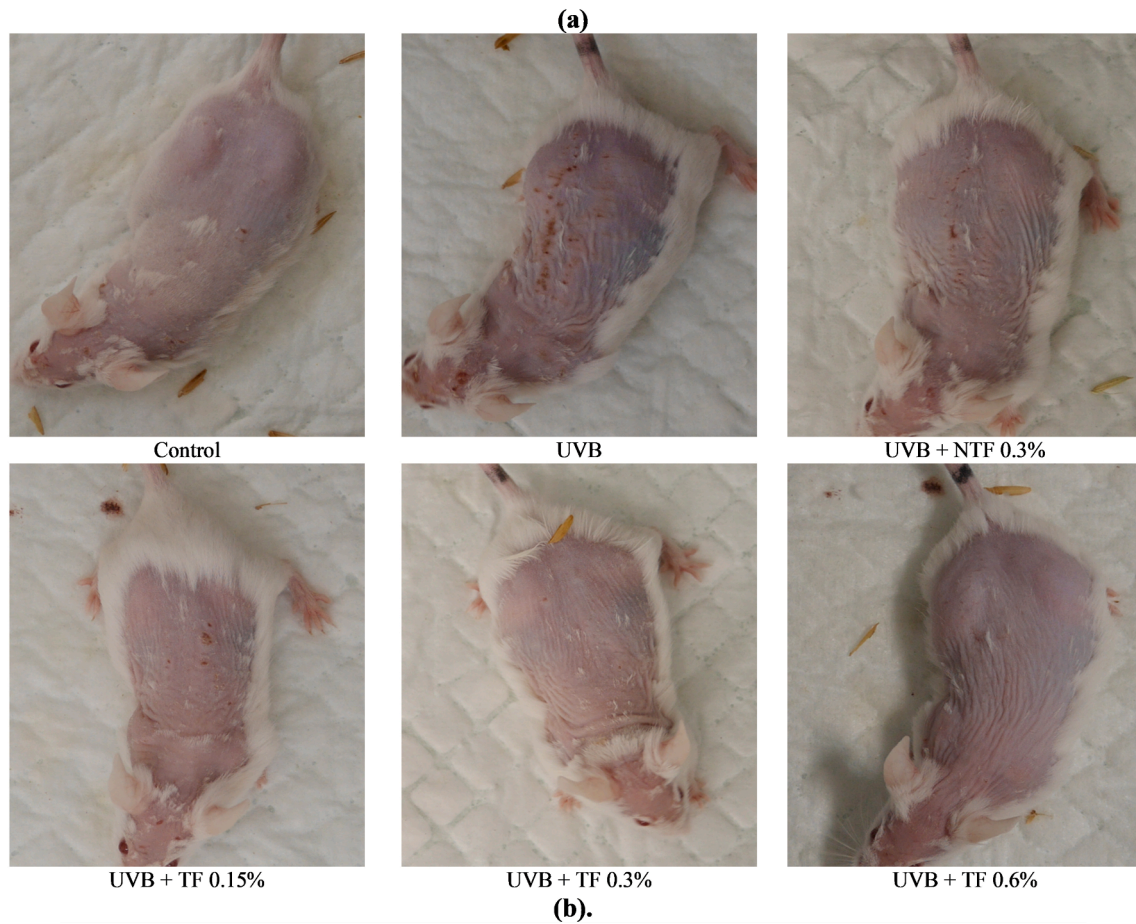


Fig. 1. Effect of CA-TF and BEO-NE combination gel on macroscopic changes. (a). Macroscopic skin appearances. (b). Wrinkles' quantitative analysis. (c). Scores of the skin visual manifestation. Data represent mean \pm SD (n = 4). The same chart's data with different notations implied significant differences at P < 0.05.

significantly ameliorated and considerably lower compared with UVB group.

3.3. Effect of CA-TF and BEO-NE combination gel on histological changes

The control group (normal), shown in Fig. 2.a appeared healthy, showing no signs of abnormal structure or inflammatory cell aggregation, thin epidermis, dermal-epidermal junction (DEJ) waves, closely

interwoven collagen bundles, and distributed elastic fibers. In response to UVB exposure, the UVB group mice skin showed almost similar features and photo-damaged skin histology, such as thickening of the epidermis, increased stratum corneum, flattened DEJ, aggregation of inflammatory cells, tangled and degraded collagen fibers, elastic fibers also degraded, which provides evidence that UVB induces photoaging in mice skin. By comparison, the topical application of CA-non-TF and BEO-NE (CA extract) combination gel ameliorated the damage to skin

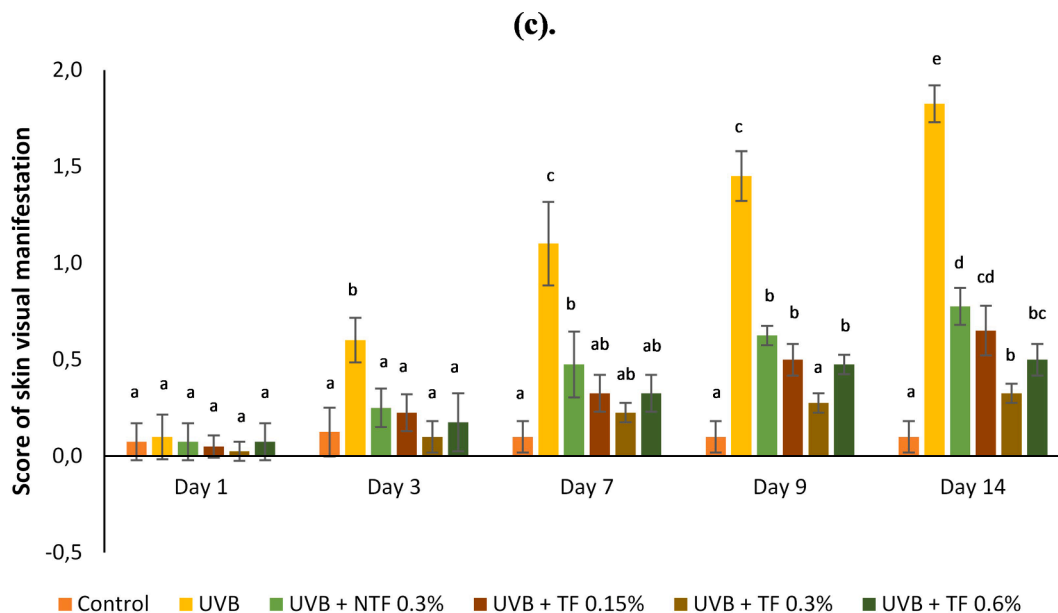


Fig. 1. (continued).

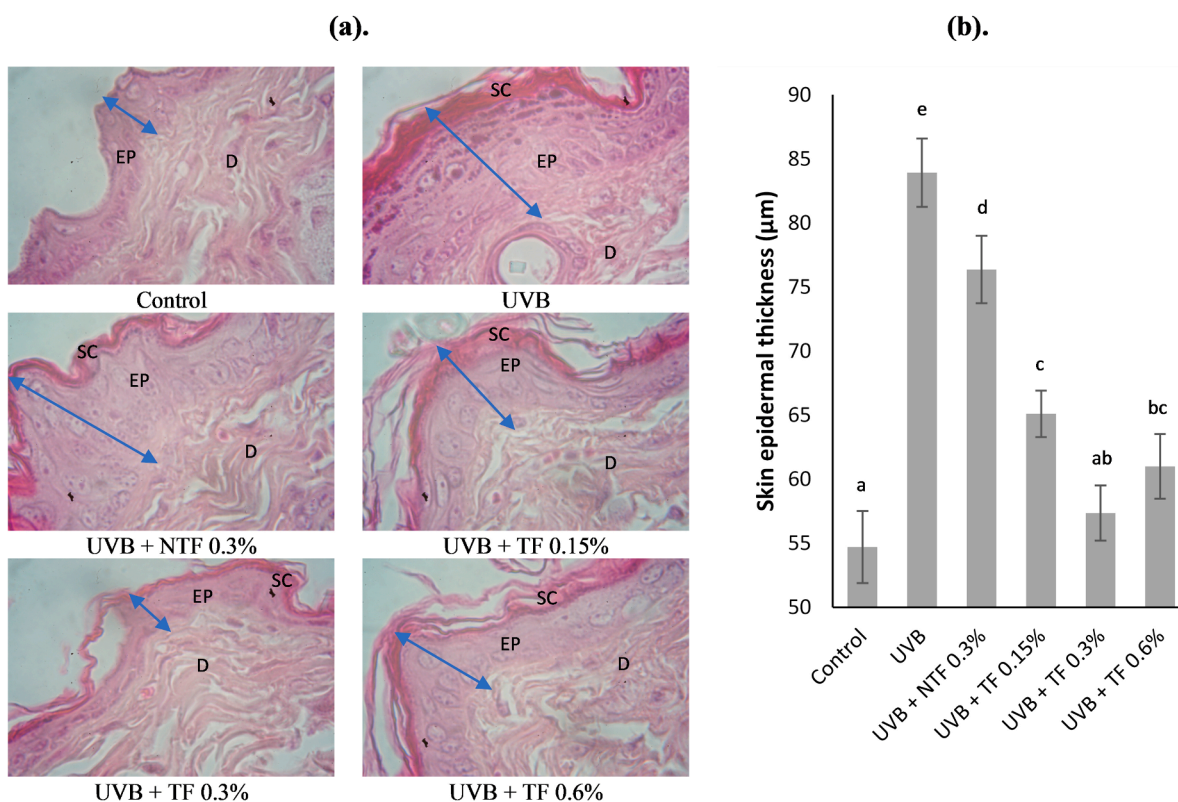


Fig. 2. Effect of CA-TF and BEO-NE combination gel on histological appearance. (a). Hematoxylin and eosin (HE) were used to stain dorsal skin slices. (b). Epidermal thicknesses quantitative analysis. Data represent mean \pm SD (n = 4). The same chart's data with different notations implied significant differences at $P < 0.05$. D: dermis; EP: epidermis; SC: stratum corneum.

structure caused by UVB exposure. In contrast, topical application of CA-TF and BEO-NE combination gel (UVB + TF 0.3 % group) exhibited the same alterations in skin histology as the control group.

As exhibited in (Fig. 2.b), the UVB group's epidermal thickness increased by 83.9 μm in comparison with control group ($p < 0.05$). However, comparing the UVB + NTF 0.3 % group with the UVB group, there was a significant decrease of 76.3 μm in epidermal thickness due to

UVB exposure. In the UVB + TF 0.15 %, 0.3 %, and 0.6 % groups, the topically applied CA-TF and BEO-NE combination gel significantly reduced the epidermal thickness by 65.1 μm , 57.3 μm , and 61.0 μm , respectively, in concentration-dependent manners.

3.4. Effect of CA-TF and BEO-NE combination gel on collagen changes

Masson's trichrome stain is one of the parameters to evaluate and visualize changes in collagen fibers in the dermal layer. As shown in Fig. 3.a, the collagen fibers in the skin tissue of the normal group are shown in the dermis, neatly arranged, evenly distributed, wavy, and bright blue. However, UVB exposure causes abnormal accumulation, disordered arrangement, laxity, and decreased collagen fiber content. After topical application of non-TF and TF groups, fragmentation and morphology of collagen fibers were ameliorated.

Fig. 3.b shows that the UVB group's quantitative assessment of collagen fiber density significantly decreased by 46.2 % when compared to the control (normal) group. This decline was defined by decreased collagen fibers stained with blue dye. In contrast, topical application with the CA-non-TF and BEO-NE combination gel (UVB + NTF 0.3 % group) improved collagen fiber density by 46.2 %. However, there was no statistically significant difference compared with the UVB group. While topical application with CA-TF and BEO-NE combination gel significantly reversed the loss of collagen fibers due to UVB exposure in all groups compared to the UVB group, UVB + TF 0.15 by 52.2 %, UVB + TF 0.3 % by 55.9 %, and UVB + TF 0.6 % by 51.8 %.

3.5. Effect of CA-TF and BEO-NE combination gel on SOD and MDA expressions

In this study, UVB-induced BALB/c mice resulted from oxidative damage, as seen with the depletion of endogenous antioxidants, through decreased SOD activity and increased lipid peroxidation products. (Fig. 4.a and 5.a). Compared with normal group, UVB group SOD expression significantly decreased by 46.74 % ($p < 0.05$) (Fig. 4.b). The UVB + NTF 0.3 % group and the UVB + TF 0.15 % and 0.6 % groups did not significantly differ in SOD expression. However, compared with UVB group, the SOD expression was much higher by 51.90 %, 56.17 %, and

52.54 %, respectively. When topically applied with CA-TF and BEO-NE combination gel (UVB + TF 0.3 % group), the SOD expression was significantly increased by 58.29 % compared with UVB group.

UVB group MDA expression significantly increased by 59.40 % compared with control group (normal) (Fig. 5.b). However, the UVB-induced MDA expression was significantly suppressed by 54.51 % in the UVB + NTF 0.3 % group compared with UVB group. When topically applied with CA-TF and BEO-NE combination gel, the expression of MDA significantly reduced considerably lower 50.49 %, 48.78 %, and 51.55 %, respectively, in UVB + TF 0.15 %, 0.3 %, and 0.6 % groups than that in the UVB group.

3.6. Effect of CA-TF and BEO-NE combination gel on TNF- α and IL-6 expressions

The expression and distribution of pro-inflammatory cytokines were determined by immunohistochemical analysis, including TNF- α and IL-6, described by brown skin signals (Figs. 6.a and Fig. 7.a). The results revealed that the UVB group's TNF- α expressions were significantly enhanced than those of the control group by 59.34 % ($p < 0.05$). Fig. 6.b shows that TNF- α expression was attenuated by 55.28 % in the UVB + NTF 0.3 % group. In addition, TNF- α expression was significantly reduced upon topically applied with CA-TF and BEO-NE combination gel (UVB + TF 0.15 %, 0.3 %, and 0.6 % groups), showing about 53.00 %, 51.60 %, and 52.90 % reduction respectively compared with UVB control group, and lower compared to the UVB + NT 0.3 % group.

Fig. 7.b shows that the uvb group expression of il-6 significantly enhanced by 58.05 % compared to the control group. However, topically applied CA-non-TF and BEO-NE combination gel (UVB + NTF 0.3 % group) UVB-induced upregulation of IL-6 expression was significantly suppressed by 52.49 %, compared with UVB group. When topically applied with CA-TF and BEO-NE combination gel, the expression of IL-6 significantly reduced considerably lower by 50.84 %, 45.81 %, and

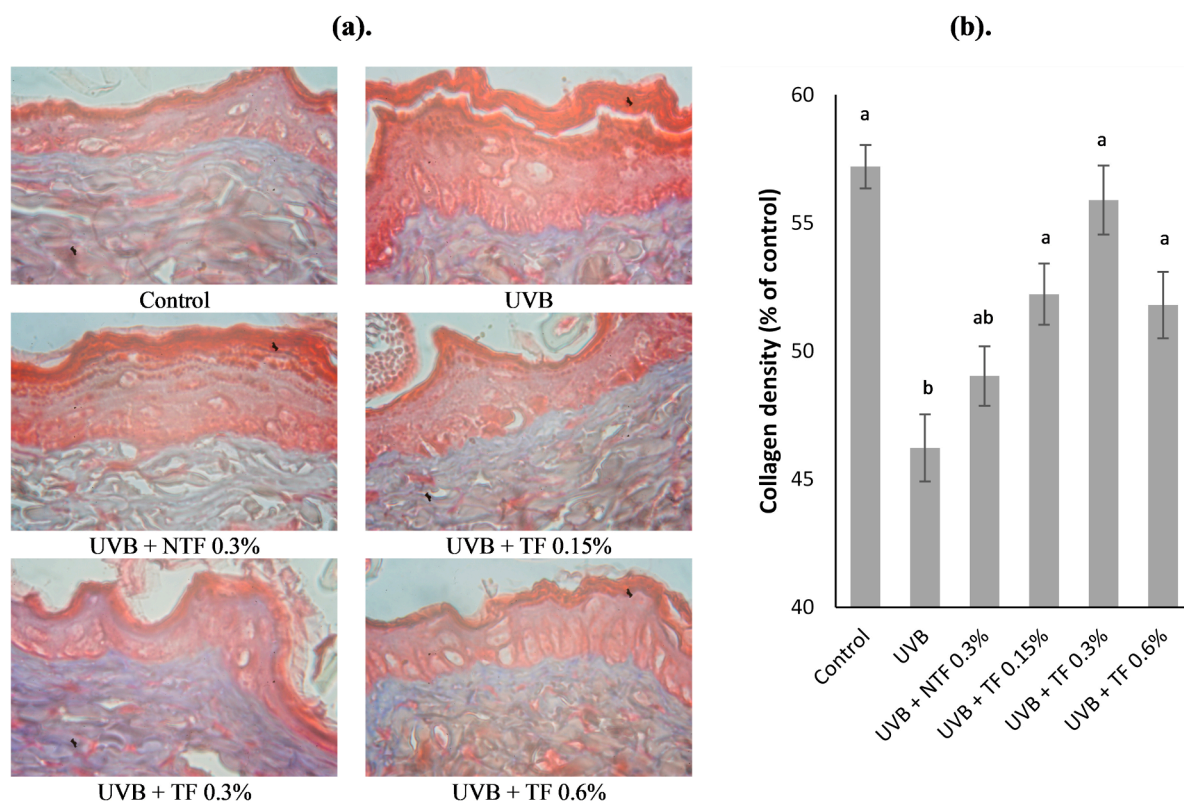


Fig. 3. Effect of CA-TF and BEO-NE combination gel on collagen fiber destruction. (a). Collagen fibers are visible with Masson's trichrome staining. (b). Collagen fiber density quantitative analysis. Data represent mean \pm SD ($n = 4$). The same chart's data with different notations implied significant differences at $P < 0.05$.

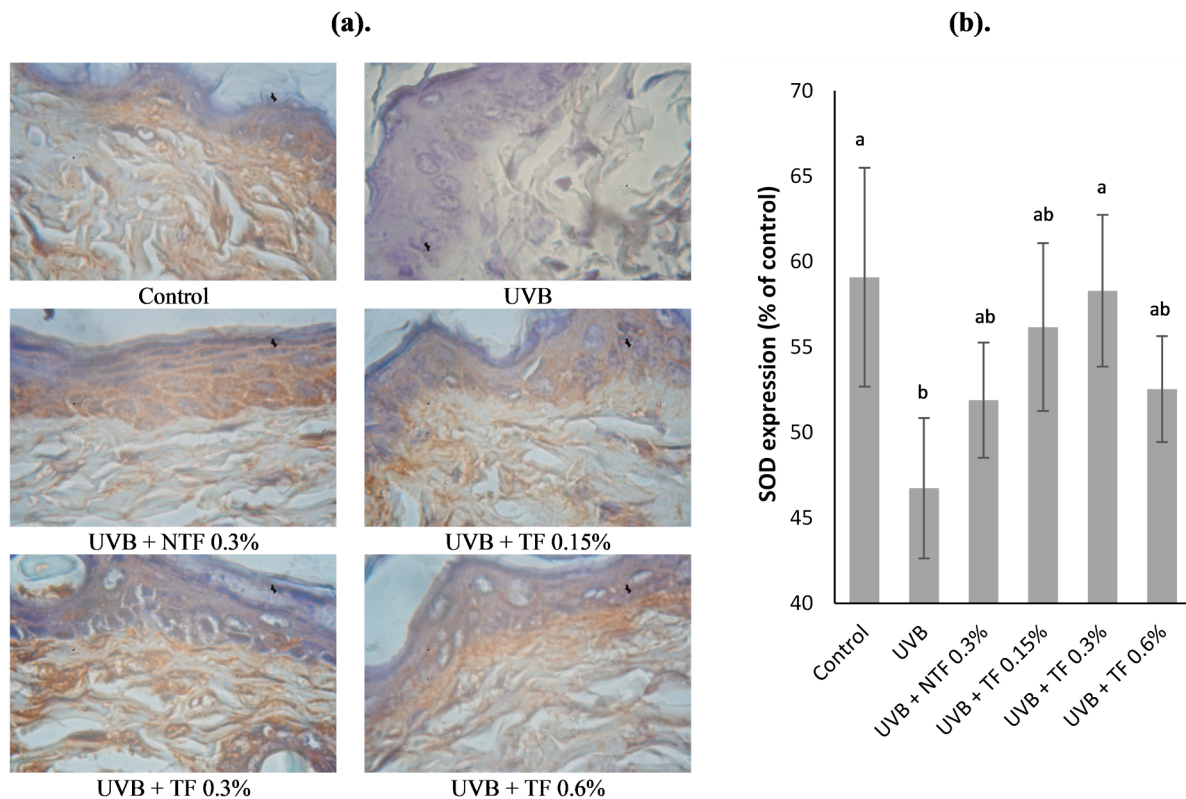


Fig. 4. Effect of CA-TF and BEO-NE combination gel on SOD expressions. (a). SOD immunohistochemistry sections. (b). SOD expression's quantitative analysis. Data represent mean \pm SD (n = 4). The same chart's data with different notations implied significant differences at P < 0.05.

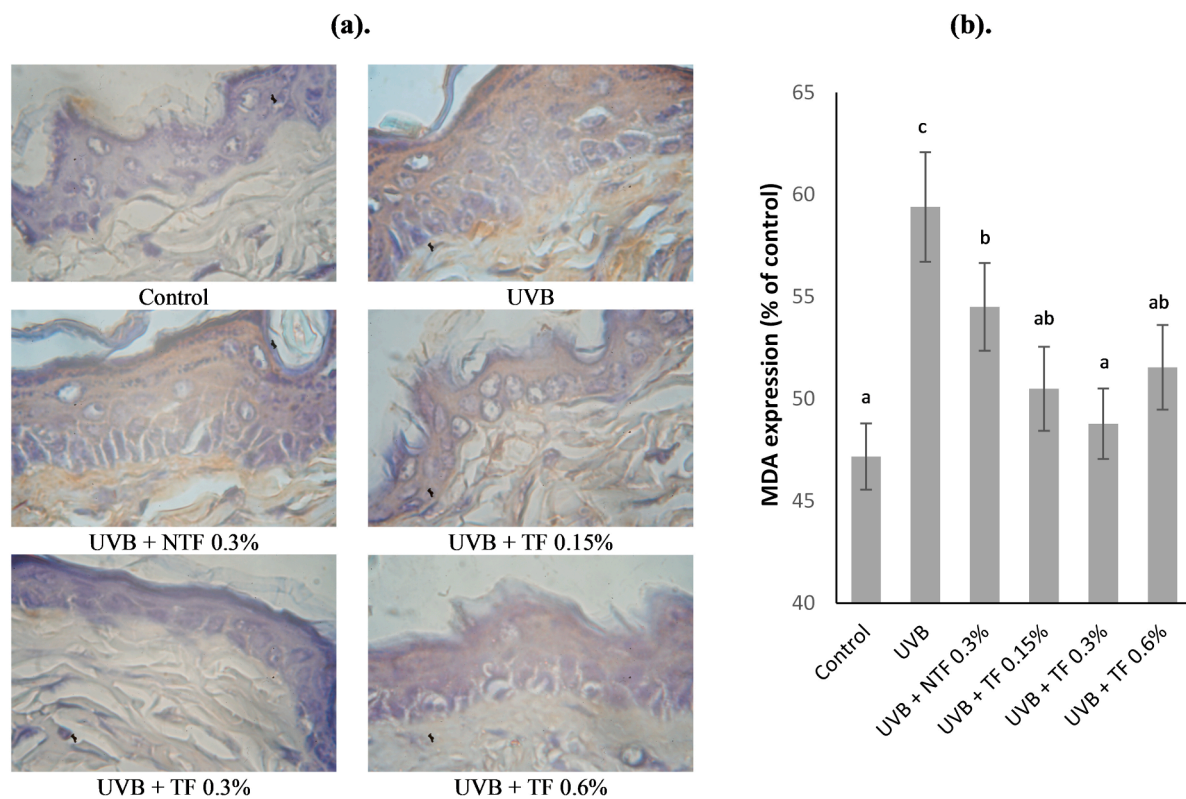


Fig. 5. Effect of CA-TF and BEO-NE combination gel on lipid peroxidation. (a). MDA immunohistochemistry sections (b). MDA expression's quantitative analysis. Data represent mean \pm SD (n = 4). The same chart's data with different notations implied significant differences at P < 0.05.

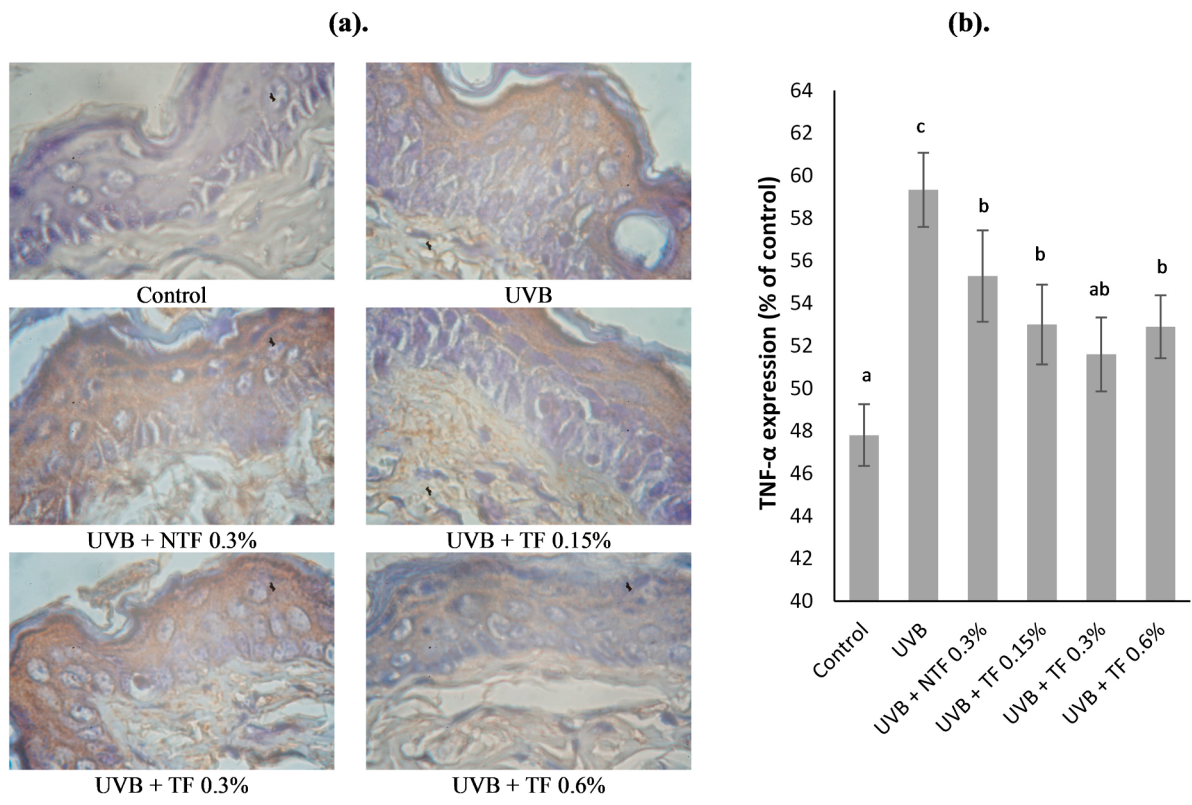


Fig. 6. Effect of CA-TF and BEO-NE combination gel on TNF- α expressions. (a). TNF- α immunohistochemistry sections. (b). TNF- α expression's quantitative analysis. Data represent mean \pm SD (n = 4). The same chart's data with different notations implied significant differences at P < 0.05.

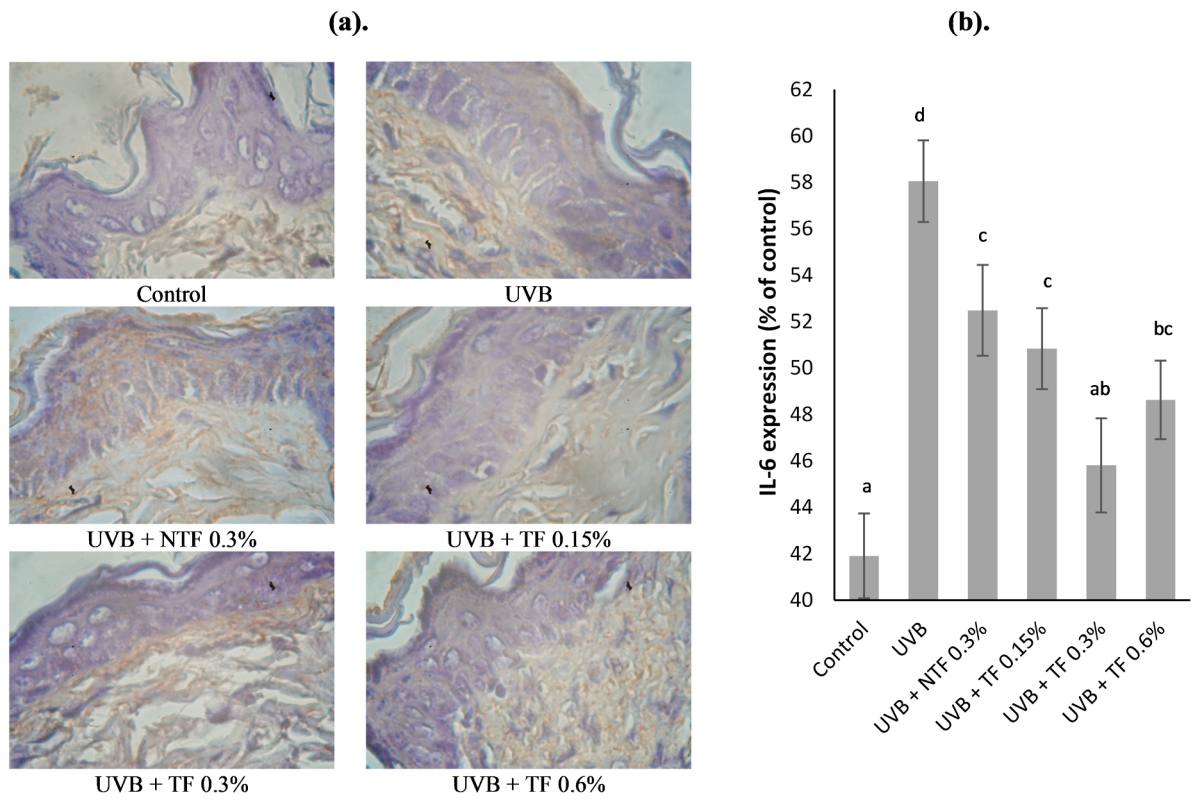


Fig. 7. Effect of CA-TF and BEO-NE combination gel on IL-6 expressions. (a). IL-6 immunohistochemistry sections. (b). IL-6 expression's quantitative analysis. Data represent mean \pm SD (n = 4). The same chart's data with different notations implied significant differences at P < 0.05.

48.63 %, respectively, at UVB + TF 0.15 %, 0.3 %, and 0.6 % groups, compared with UVB group.

3.7. Effect of CA-TF and BEO-NE combination gel on type I collagen expression

UVB-induced type I collagen expression can be significantly suppressed, as shown in Fig. 8.b. This is a major factor in UVB-induced skin photoaging. Compared with normal group, UVB group type I collagen expression significantly decreased by 44.29 % ($p < 0.05$). While topically applied with CA non-TF and BEO-NE combination gel, the skin of mice showed that type I collagen expression did not significantly increase compared to the UVB group. However, in the UVB + NTF 0.3 %, UVB + TF 0.15 %, and 0.6 % groups, the expression of type I collagen was much higher compared to the UVB group at 48.18 %, 51.95 %, and 51.82 %, respectively. When topically applied with CA-TF and BEO-NE combination gel (UVB + TF 0.3 % group), the type I collagen expression was significantly increased by 54.07 % compared with UVB group.

4. Discussion

Interest in skincare products grows with people's life expectancy. Research has been conducted and committed to addressing skin health and beauty, especially in preventing skin aging (Zhang and Duan, 2018). It is well known that the skin is a complex organ with three primary layers: the hypodermis, dermis, and epidermis each of which has distinct components and functions (Lai et al., 2020). The smaller the particle size of a colloidal formula, the greater the contact between the active ingredients of that formula and the stratum corneum of the skin pores, thereby increasing the penetration of the active substances into the dermis. In this work, CA and BEO were encapsulated in TF and NE, respectively, showing an average particle size pattern in the nano range (<100 nm) with a polydispersity index < 0.2 . The polydispersity index was used to measure the uniformity of particle size, where the

nanocarriers with a smaller polydispersity index showed a good size distribution, while a higher polydispersity index indicated low size uniformity of nanocarriers (Sharma et al., 2019). The zeta potential is also an essential parameter for determining the total surface charge of particles, the interactions between particles, and reflecting their long-term stability, as well as predicting the tendency of particles to aggregate (Khan et al., 2022). Our results show that the encapsulated CA-TF and BEO-NE formulations have negative charges, with zeta potential values -39.86 ± 1.33 mV, indicating low aggregation probability and high stability.

It is well known that the skin photoaging process is caused by prolonged exposure to UVB radiation, manifested by the dryness formation, roughness, wrinkling, and laxity of the skin, which is related to a decrease in collagen and elastic fibers content (Lee et al., 2018). Degradation and destruction of collagen in the dermis, particularly in the major structural components of the ECM, is a major cause of photodamage (Kong et al., 2018). According to previous reports, clinical observations and macroscopic grading indicated that UVB exposure causes increased wrinkle formation and skin thickness and decreased skin elasticity (Feng et al., 2014; Xian et al., 2017). Typical photoaging features, including dryness, roughness, erythema, coarse wrinkles, and laxity in macroscopic appearance, were observed in this study. Histological observations revealed that the UVB-induced mice skin has increased epidermal hyperplasia, tangled elastic fibers, and disorganized and degraded bundles. Additionally, UVB-induced skin photoaging significantly reduces the density of collagen fibers. However, topically applied CA-TF and BEO-NE combination gel could act synergistically and significantly to reduce adverse changes, including the formation of skin wrinkles, increased epidermis thickness, and degradation of elastin and collagen fibers in skin tissue exposed to UVB.

Skin photoaging by UVB is characterized by an imbalance between the number of free radicals and antioxidants, resulting in oxidative stress and increased levels of intracellular ROS (Bosch et al., 2015). Under physiological conditions, endogenous antioxidant systems, such as SOD,

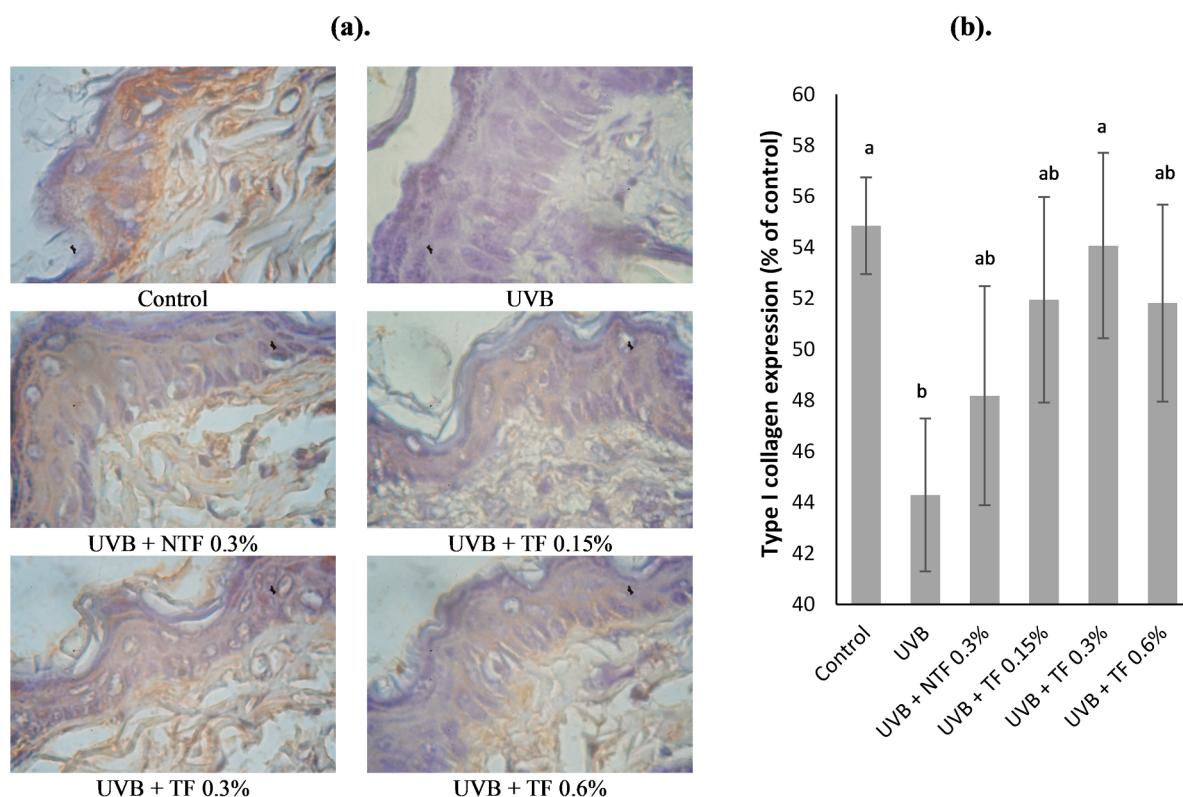


Fig. 8. Effect of CA-TF and BEO-NE combination gel on type I collagen expressions. (a). Type I collagen's immunohistochemistry sections. (b). Type I collagen expression's quantitative analysis. Data represent mean \pm SD ($n = 4$). The same chart's data with different notations implied significant differences at $P < 0.05$.

CAT, and GSH-Px can typically scavenge to maintain enzymatic and non-enzymatic antioxidant levels in ideal balance and to maintain MMPs expression at low physiological levels. However, when ROS production is excessive by UVB exposure, endogenous antioxidant enzyme functions are overwhelmed, leading to oxidative stress and skin damage (Pandel et al., 2013). In previous studies, exposure to UVB dramatically reduced the antioxidant enzyme activity while increasing the generation of MDA (Si et al., 2019). MDA is an end-product and a major bioactive marker of lipid peroxidation, indicating oxidative damage to cells and tissues (Cho et al., 2018); therefore, we confirmed this by macroscopic and histological evaluation. Our results demonstrate that UVB radiation significantly reduces SOD activity while dramatically increasing the MDA formation.

Excessive free radicals due to UVB radiation can activate the AP-1, NF- κ B and MAPK signaling pathways, this will affect various biological processes, including inflammation known as the central effector of photoaging (Wang et al., 2019). The mechanism of inflammation caused by UVB exposure initiates with the release of pro-inflammatory cytokines, including IL-1 from the stratum corneum, activation of TNF- α synthesis, and release from keratinocytes. These two primary cytokines stimulate the production and release of other pro-inflammatory cytokines in response to UVB exposure (Auh and Madhavan, 2021). Histological analysis with HE staining revealed many inflammatory cells in and beneath the dermis, consistent with the macroscopic appearance of photoaged mice skin. These results were further confirmed by the expression of TNF- α and IL-6, which are NF- κ B and MMPs activators and contribute to the loss of interstitial collagen in photoaged skin. IL-6 is a general inflammatory marker closely related to chronic disease and has pro-inflammatory properties. TNF- α contributes to the chemotaxis of inflammatory cells into the skin, which secretes elastase and collagenase, causing skin photoaging. It releases cytokines, chemokines, and adhesion molecules (Nakajima et al., 2012).

The primary constituent of the ECM and a crucial marker of skin photoaging, collagen contributes to maintaining the skin's structural integrity and physiological function. Especially type I collagen, accounting for 70 % of the generous layer in the skin's dermis, is essential for maintaining skin elasticity, firmness, and resistance to aging, but its production declines with age (Shin et al., 2019; Reilly and Lozano, 2021). UVB exposure contributes to the formation of ROS, which in turn activates the MAPK pathway and induces the AP-1 transcription factor; this further induces MMP-1 synthesis. It is well known that MMP-1 plays a role as the main enzyme in type I collagen degradation in skin photoaging (Pittayapruek et al., 2016). Decreased type I collagen expression is a histological characteristic for evaluating skin photoaging. The CA-TF and BEO-NE combined gels topically applied can effectively reverse UVB-induced skin (Figure 8). In particular, CA-TF and BEO-NE have been shown to restore the balance between collagen degeneration and collagen synthesis disrupted by UVB exposure. Overall, we hope these findings will be one of the beneficial ingredients inhibiting the formation of wrinkles.

5. Conclusion

This study demonstrated that the synergistic effect of nanocarriers CA-TF and BEO-NE combined with a gel formulation has been successfully developed and acts as an alternative topical drug delivery system to prevent and protect against UVB radiation in anti-photoaging effects. The physicochemical characteristics of CA-TF and BEO-NE exhibited small particle sizes with narrow polydispersity index and negative zeta potential. Topically applied CA-TF and BEO-NE gel combinations effectively protect the skin's UVB-induced macroscopic and histological appearance, especially by inhibiting oxidative stress and inflammatory response while enhancing antioxidant activity and collagen synthesis.

CRedit authorship contribution statement

Ekowati Retnaningtyas: Conceptualization, Data curation, Formal analysis, Funding acquisition, Investigation, Methodology, Project administration, Resources, Software, Supervision, Validation, Visualization, Writing – original draft, Writing – review & editing. **Budi Susatia:** Investigation, Project administration, Supervision, Validation, Visualization, Writing – original draft, Writing – review & editing, Resources. **Husnul Khotimah:** Data curation, Formal analysis, Investigation, Methodology, Project administration, Supervision, Validation, Visualization, Writing – original draft, Writing – review & editing, Resources. **Achmad Rudijanto:** Investigation, Project administration, Resources, Supervision, Validation, Visualization, Writing – original draft, Writing – review & editing. **Ahmed Ali Ahmed Abousouh:** Data curation, Formal analysis, Investigation, Visualization, Writing – original draft, Writing – review & editing, Methodology, Validation. **Andri Setiawan:** Data curation, Formal analysis, Investigation, Methodology, Project administration, Software, Supervision, Validation, Writing – original draft, Writing – review & editing, Visualization.

Declaration of competing interest

The authors declare that they have no known competing financial interests or personal relationships that could have appeared to influence the work reported in this paper.

Acknowledgement

This research was supported by the health workforce development research (Risbinakes), Malang State Health Polytechnic, Ministry of Health Republic of Indonesia (HK.03.01/1/2110/2022).

References

- Ansary, T.M., Hossain, M.R., Kamiya, K., Komine, M., Ohtsuki, M., 2021. Inflammatory molecules associated with ultraviolet radiation-mediated skin aging. *Int. J. Mol. Sci.* 22 <https://doi.org/10.3390/ijms22083974>.
- Auh, J.H., Madhavan, J., 2021. Protective effect of a mixture of marigold and rosemary extracts on UV-induced photoaging in mice. *Biomed. Pharmacother.* 135, 111178 <https://doi.org/10.1016/j.biopha.2020.111178>.
- Belwal, T., Andola, H.C., Atanassova, M.S., Joshi, B., Suyal, R., Thakur, S., Bisht, A., Jantwal, A., Bhatt, I.D., Rawal, R.S., 2019. Gotu Kola (*Centella asiatica*), in: *Nonvitamin and Nonmineral Nutritional Supplements*. Elsevier, pp. 265–275. [Doi: 10.1016/B978-0-12-812491-8.00038-2](https://doi.org/10.1016/B978-0-12-812491-8.00038-2).
- Bilia, A.R., Guccione, C., Isacchi, B., Righeschi, C., Firenzuoli, F., Bergonzi, M.C., 2014. Essential oils loaded in nanosystems: a developing strategy for a successful therapeutic approach. *Evidence-Based Complement. Altern. Med.* 1–15 <https://doi.org/10.1155/2014/651593>.
- Bosch, R., Philips, N., Suárez-Pérez, J.A., Juarranz, A., Devmurari, A., Chalensouk-Khaosaat, J., González, S., 2015. Mechanisms of photoaging and cutaneous photocarcinogenesis, and photoprotective strategies with phytochemicals. *Antioxidants*. <https://doi.org/10.3390/antiox4020248>.
- Bylka, W., Znajdek-Awiżeń, P., Studzińska-Sroka, E., Dańczak-Pazdrowska, A., Brzezińska, M., 2014. *Centella asiatica* in dermatology: an overview. *Phyther. Res.* 28, 1117–1124. <https://doi.org/10.1002/ptr.5110>.
- Dugo, G., Bonaccorsi, I., 2013. *Citrus bergamia*. CRC Press. <https://doi.org/10.1201/b15375>.
- El Zaafarany, G.M., Awad, G.A.S., Holayel, S.M., Mortada, N.D., 2010. Role of edge activators and surface charge in developing ultradeformable vesicles with enhanced skin delivery. *Int. J. Pharm.* 397, 164–172. <https://doi.org/10.1016/j.ijpharm.2010.06.034>.
- El-Gizawy, S.A., Nouh, A., Saber, S., Kira, A.Y., 2020. Deferoxamine-loaded transferrin accelerates healing of pressure ulcers in streptozotocin-induced diabetic rats. *J. Drug Deliv. Sci. Technol.* 58, 101732 <https://doi.org/10.1016/j.jddst.2020.101732>.
- Feng, X.X., Yu, X.T., Li, W.J., Kong, S.Z., Liu, Y.H., Zhang, X., Xian, Y.F., Zhang, X.J., Su, Z.R., Lin, Z.X., 2014. Effects of topical application of patchouli alcohol on the UV-induced skin photoaging in mice. *Eur. J. Pharm. Sci.* 63, 113–123. <https://doi.org/10.1016/j.ejps.2014.07.001>.
- Gu, Y., Han, J., Jiang, C., Zhang, Y., 2020. Biomarkers, oxidative stress and autophagy in skin aging. *Ageing Res. Rev.* 59, 101036 <https://doi.org/10.1016/j.arr.2020.101036>.
- Hoang, H.T., Moon, J.Y., Lee, Y.C., 2021. Natural antioxidants from plant extracts in skincare cosmetics: recent applications, challenges and perspectives. *Cosmetics* 8, 1–24. <https://doi.org/10.3390/cosmetics8040106>.

- Kammeyer, A., Luiten, R.M., 2015. Oxidation events and skin aging. *Ageing Res. Rev.* 21, 16–29. <https://doi.org/10.1016/j.arr.2015.01.001>.
- Keskin, I., Gunal, Y., Ayla, S., Kolbasi, B., Sakul, A., Kilic, U., Gok, O., Koroglu, K., Ozbek, H., 2017. Effects of *Poeniciculum vulgare* essential oil compounds, fenchone and limonene, on experimental wound healing. *Biotech. Histochem.* 92, 274–282. <https://doi.org/10.1080/10520295.2017.1306882>.
- Khan, M.L., Yaqoob, S., Madni, A., Akhtar, M.F., Sohail, M.F., Saleem, A., Tahir, N., Khan, K.U.R., Qureshi, O.S., 2022. Development and in vitro/ex vivo evaluation of lecithin-based deformable transfersomes and transfersome-based gels for combined dermal delivery of Meloxicam and dexamethasone. *Biomed. Res. Int.* 2022, 8170318. <https://doi.org/10.1155/2022/8170318>.
- Khotimah, H., Setiawan, A., Rita, C.I., Mardiyah, M., Ali, A., Sukatman, M.P., Retnaningtyas, E., Ismail, D.D.S.L., Widasmara, D., Nurseta, T., Sujuti, H., 2021. In silico studies of natural compounds of *Centella asiatica* as anti-aging and wound healing agents. In: INTERNATIONAL CONFERENCE ON LIFE SCIENCES AND TECHNOLOGY (ICoLiST 2020). p. 030031. Doi: 10.1063/5.0053016.
- Khotimah, H., Aulanni'am, A., Nandar Kurniawan, S., Eka Puspita, O., Rahayu Adianingsih, O., Mardiyah, M., Setiawan, A., 2022a. Development and optimization of orally disintegrating tablets containing *Centella asiatica* solid lipid nanoparticles for supportive therapies of Parkinson's disease. *F1000Research* 11, 517. Doi: 10.12688/f1000research.118951.1.
- Khotimah, H., Dewi Lestari Ismail, D., Riawan, W., Retnaningtyas, E., Weka Nugraheni, R., Eka Puspita, O., Rahayu Adianingsih, O., Mardiyah, M., Setiawan, A., 2022b. Ameliorative effect of gel combination of *Centella asiatica* extract transfersomes and rosemary essential oil nanoemulsion against UVB-induced skin aging in Balb/c mice. *F1000Research* 11, 288. Doi: 10.12688/f1000research.109318.1.
- Kong, S.Z., Li, D.D., Luo, H., Li, W.J., Huang, Y.M., Li, J.C., Hu, Z., Huang, N., Guo, M.H., Chen, Y., Li, S.D., 2018. Anti-photoaging effects of chitosan oligosaccharide in ultraviolet-irradiated hairless mouse skin. *Exp. Gerontol.* 103, 27–34. <https://doi.org/10.1016/j.exger.2017.12.018>.
- Krutmann, J., Schikowski, T., Morita, A., Berneburg, M., 2021. Environmentally-induced (extrinsic) skin aging: exposomal factors and underlying mechanisms. *J. Invest. Dermatol.* 141, 1096–1103. <https://doi.org/10.1016/j.jid.2020.12.011>.
- Lai, F., Caddeo, C., Manca, M.L., Manconi, M., Sinico, C., Fadda, A.M., 2020. What's new in the field of phospholipid vesicular nanocarriers for skin drug delivery. *Int. J. Pharm.* 583, 119398. <https://doi.org/10.1016/j.ijpharm.2020.119398>.
- Laronha, H., Caldeira, J., 2020. Structure and function of human matrix metalloproteinases. *Cells* 9, 1076. <https://doi.org/10.3390/cells9051076>.
- Lawrence, K.P., Douki, T., Sarkany, R.P.E., Acker, S., Herzog, B., Young, A.R., 2018. The UV/Visible radiation boundary region (385–405 nm) damages skin cells and induces "dark" cyclobutane pyrimidine Dimers in human skin in vivo. *Sci. Rep.* 8, 1–12. <https://doi.org/10.1038/s41598-018-30738-6>.
- Lee, H.J., Im, A.-R., Kim, S.-M., Kang, H.-S., Lee, J.D., Chae, S., 2018. The flavonoid hesperidin exerts anti-photoaging effect by downregulating matrix metalloproteinase (MMP)-9 expression via mitogen activated protein kinase (MAPK)-dependent signaling pathways. *BMC Complement. Altern. Med.* 18, 39. <https://doi.org/10.1186/s12906-017-2058-8>.
- Maisel, A., Waldman, A., Furlan, K., Weil, A., Sacotte, K., Lazaroff, J.M., Lin, K., Aranzazu, D., Avram, M.M., Bell, A., Cartee, T.V., Cazzaniga, A., Chapas, A., Crispin, M.K., Croix, J.A., Digiorgio, C.M., Dover, J.S., Goldberg, D.J., Goldman, M. P., Green, J.B., Griffin, C.L., Haimovic, A.D., Hausauer, A.K., Hernandez, S.L., Hsu, S., Ibrahim, O., Jones, D.H., Kaufman, J., Kilmer, S.L., Lee, N.Y., McDaniel, D. H., Schlessinger, J., Tanzi, E., Weiss, E.T., Weiss, R.A., Wu, D., Poon, E., Alam, M., 2018. Self-reported patient motivations for seeking cosmetic procedures. *JAMA Dermatol.* 154, 1167–1174. <https://doi.org/10.1001/jamadermatol.2018.2357>.
- Mishra, D.K., Shandilya, R., Mishra, P.K., 2018. Lipid based nanocarriers: a translational perspective. *nanomedicine nanotechnology. Biol. Med.* 14, 2023–2050. <https://doi.org/10.1016/j.nano.2018.05.021>.
- Nakajima, H., Yoshioka, R., Ezaki, Y., Nagai, T., Imokawa, G., 2012. Paracrine cytokine interaction between UVB-exposed epidermal keratinocytes and dermal fibroblasts in stimulating expression of skin fibroblast-derived elastase. *Cytokine* 59, 166–175. <https://doi.org/10.1016/j.cyto.2012.03.008>.
- Naseema, A., Kovooru, L., Behera, A.K., Kumar, K.P.P., Srivastava, P., 2021. A critical review of synthesis procedures, applications and future potential of nanoemulsions. *Adv. Colloid Interface Sci.* 287, 102318. <https://doi.org/10.1016/j.cis.2020.102318>.
- Pandel, R., Poljšak, B., Godic, A., Dahmane, R., 2013. Skin photoaging and the role of antioxidants in its prevention. *ISRN Dermatol.* 1–11. <https://doi.org/10.1155/2013/930164>.
- Perna, S., Spadaccini, D., Botteri, L., Girometta, C., Riva, A., Allegrini, P., Petrangolini, G., Infantino, V., Rondanelli, M., 2019. Efficacy of bergamot: From anti-inflammatory and anti-oxidative mechanisms to clinical applications as preventive agent for cardiovascular morbidity, skin diseases, and mood alterations. *Food Sci. Nutr.* Doi: 10.1002/fsn3.903.
- Pittayapruek, P., Meephansan, J., Prapapan, O., Komine, M., Ohtsuki, M., 2016. Role of matrix metalloproteinases in photoaging and Photocarcinogenesis. *Int. J. Mol. Sci.* 17, 1–20. <https://doi.org/10.3390/ijms17060868>.
- Reilly, D.M., Lozano, J., 2021. Skin collagen through the lifestages: importance for skin health and beauty. *Plast. Aesthetic Res.* 2021. <https://doi.org/10.20517/2347-9264.2020.153>.
- Sharma, B., Iqbal, B., Kumar, S., Ali, J., Baboota, S., 2019. Resveratrol-loaded nanoemulsion gel system to ameliorate UV-induced oxidative skin damage: from in vitro to in vivo investigation of antioxidant activity enhancement. *Arch. Dermatol. Res.* 311, 773–793. <https://doi.org/10.1007/s00403-019-01964-3>.
- Shin, J.W., Kwon, S.H., Choi, J.Y., Na, J.I., Huh, C.H., Choi, H.R., Park, K.C., 2019. Molecular mechanisms of dermal aging and antiaging approaches. *Int. J. Mol. Sci.* 20. <https://doi.org/10.3390/ijms20092126>.
- Shukla, T., Upmanyu, N., Prakash Pandey, S., Gosh, D., 2018. Lipid nanocarriers, Lipid Nanocarriers for Drug Targeting. Elsevier Inc. Doi: 10.1016/B978-0-12-813687-4.00001-3.
- Si, Y., Liu, W., McClements, D.J., Chen, X., Hu, Z., Zou, L., 2019. Ameliorative effects of snake (*Deinagkistrodon acutus*) oil and its main fatty acids against UVB-induced skin photodamage in mice. *J. Photochem. Photobiol. B Biol.* 197, 111538. <https://doi.org/10.1016/j.jphotobiol.2019.111538>.
- Souto, E.B., Cano, A., Martins-Gomes, C., Coutinho, T.E., Zielińska, A., Silva, A.M., 2022. Microemulsions and nanoemulsions in skin drug delivery. *Bioengineering* 9, 1–22. <https://doi.org/10.3390/bioengineering9040158>.
- Sun, B., Wu, L., Wu, Y., Zhang, C., Qin, L., Hayashi, M., Kudo, M., Gao, M., Liu, T., 2020. Therapeutic potential of *Centella asiatica* and its triterpenes: a review. *Front. Pharmacol.* 11, 1–24. <https://doi.org/10.3389/fphar.2020.568032>.
- Wang, Y., Wang, L., Wen, X., Hao, D., Zhang, N., He, G., Jiang, X., 2019. NF-κB signaling in skin aging. *Mech. Ageing Dev.* 184, 111160. <https://doi.org/10.1016/j.mad.2019.111160>.
- Xian, D., Gao, X., Xiong, X., Xu, J., Yang, L., Pan, L., Zhong, J., 2017. Photoprotection against UV-induced damage by skin-derived precursors in hairless mice. *J. Photochem. Photobiol. B Biol.* 175, 73–82. <https://doi.org/10.1016/j.jphotobiol.2017.08.027>.
- Zhang, S., Duan, E., 2018. Fighting against skin aging: the way from bench to bedside. *Cell Transplant.* 27, 729–738. <https://doi.org/10.1177/0963689717725755>.